Parallel Elastic Actuation for Efficient Large Payload Locomotion

Fabian Günther[1], Yafeng Shu[2] and Fumiya Iida[1]

***Abstract*— For legged devices, their ability of carrying payload is a necessity for a wide range of tasks. In this paper, we present a new approach of carrying payload by using a parallel elastic mechanism, which is able to carry payloads at least 3 times of its bodyweight. Although the robot has no sensory feedback and consists of only two rigid bodies and one spring loaded joint, it is able to achieve efficient and stable forward hopping for a wide range of attached payload. The presented payload carrier ETH Cargo is based on the further development of our platform CHIARO for the payload range between 0 and 100kg. After parameter optimizing using simulations, a series of real world experiments prove stable and high efficiency hopping of the prototype over a wide range of payloads.**

I. INTRODUCTION

Transportation of external payload confronts legged robots with a series of significant challenges. Apart from the changes in natural dynamics and the additional load to the actuators, additional payload influences the energy efficiency of the system. In this paper, we propose the passive dynamic payload carrier *ETH Cargo* to investigate the role of energy efficiency in legged payload transportation. In addition to its ability to carry payload up to multiple times of its own bodyweight, ETH Cargo is able to hop freely without external beam support. Containing of only two rigid bodies connected with a spring loaded joint, this design is one of the simplest possible to do so. By adding a circular foot with adequate radius, the design shows stable hopping over a wide range of parameters, which makes it suitable for carrying payload. The adaptation to different payloads does not require any changes on the mechanics, since all adjustments necessary can be done by changing amplitude and frequency of the joint actuator.

In the past, many successful passive dynamic walkers [1], [2], [3], and runners [4], [5], where developed. But since all of them are very sensitive to design parameters, they are not suitable for transporting varying payload. By making use curved feet, the stable parameter region for various SLIP-Model designs [6], [7], had been increased significantly. Open loop hip torque actuation, also called *clock torque actuation* [8] provides a simple actuation scheme which is able to further improve stability performance. And finally, the hopping monoped design allows for simple mechanical realizations [4], [9].

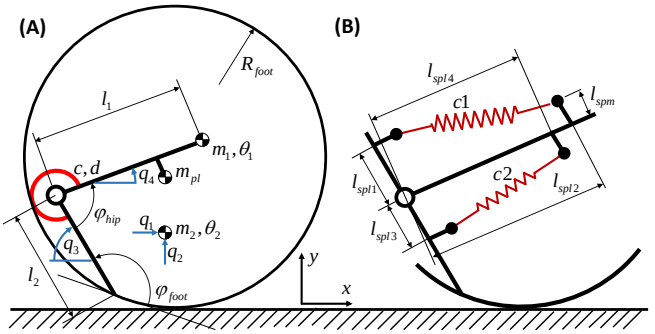

Fig. 1. **(A)** Illustration of the physical model of the ETH Cargo used for simulations. The State variables $q_1 ... q_4$ are indicated in blue. **(B)** Tension spring mechanism of the prototype.

For efficient payload carriers, the ability of storing the negative work of each gait cycle is crucial. To support the payload mass, the use of parallel elastic actuation provides an interesting option. Explored in the past for manipulation [10] and locomotion [11], [12], [13], parallel elastic actuators allow for a decoupling of the actuator from the gravitational loads of the body mass since the parallel springs can absorb the loads completely. The actuator can be used only for energy input to compensate for damping, friction and impact losses during the run.

Continuous hopping without beam support needs carefully timed swing leg motions during flight. By combining clock torque actuation, a leant forward trunk [14] with curved foot and a parallel elastic mechanism on the rotary joint, open loop forward hopping was successfully demonstrated by [15].

This paper aims to gain basic insights into payload carrying with parallel elastic mechanisms and is structured as follows. Section II describes the basic design and physical modelling of the robot. The simulation setup is explained in section III while section IV presents simulation results to find the optimal joint stiffness. Section V describes the design of the experimental platform which is used in section VI to confirm the simulation results and measure the payload carrying performance. Finally, section VII concludes the paper.

II. DESIGN AND MODELLING

The ETH Cargo presented in this paper bases on the robot CHIARO which is described in [15]. In this section, we recapitulate some of the previous work of which is important for the development of ETH Cargo. For a detailed description of the concept, the reader may refer to [15].

*This study was supported by the Swiss National Science Foundation Grant No. PP00P2123387/1 and the Swiss National Science Foundation through the National Centre of Competence in Research Robotics.

[1]F. Günther and F. Iida are with Machine Intelligence Laboratory, Department of Engineering, University of Cambridge, Trumpington Street, CB2 1PZ, Cambridge UK and with Bio-Inspired Robotics Lab, Institute of Robotics and Intelligent Systems, ETH Zurich, Leonhardstrasse 21, 8092 Zurich, Switzerland, Email fsg23@cam.ac.uk, fumiya.iida@eng.cam.ac.uk

[2]Y. Shu is with Bio-Inspired Robotics Lab, Institute of Robotics and Intelligent Systems, ETH Zurich, Leonhardstrasse 21, 8092 Zurich, Switzerland, Email: yshu@ethz.ch,

TABLE I

SELECTED PARAMETERS

Robot Parameters		
Variable	**Name**	**Value**
A_{mot}	Motor torque amplitude	[0..500]Nm
R_{foot}	Foot Radius	0.42 m
c	Rotational spring stiffness in hip joint	[1100..4400] Nm/rad
d	Damping coefficient of the hip joint	1.3 N m s
l_1	Upper body length	0.350 m
l_2	Lower body length	0.273 m
m_1	Upper body mass	15.800 kg
m_2	Lower body mass	12.802 kg
ϵ_N	Normal restitution factor between foot and ground	0
η_{gear}	Efficiency of the Gearbox	0.8
f_{mot}	Motor torque angular frequency	0 Hz to 10 Hz
m_p	Payload mass	0 kg to 100 kg
μ	Ground friction coefficient (plywood on MDF)	0.23
φ_{foot}	Foot angle	1 rad
φ_{hip}	Initial hip angle for relaxed spring	1.75 rad
Additinal Simulation Parameters		
Δt_{sim}	Simulation time step	0.025 ms to 0.5 ms
n	Number of contact points of the foot circle	78

A. Physical Model

To explore its capacity of carrying payload, we extended the simulation model of CHIARO. In parallel, we build a CAD model of ETH Cargo to provide realistic inertias and masses for the simulation. During that process, the CAD model was tested continuously for structural stability to ensure that the real robot will be able to withstand the high loads during operation.

The planar robot model of the ETH Cargo is shown in Fig. 1. It consists of two rigid bodies which are connected with a rotational hip joint on which a torsional spring is attached. Joint and motor gear friction are modelled by a linear rotational damper in the joint. A curved foot is attached to the lower body to ensure ground contact during stance phase. On the joint, a sinusoidal motor torque is applied:

$$T_{mot}(t) = A_{mot} \cdot \sin(\omega_{mot} \cdot t). \tag{1}$$

The electric power input into the motor is calculated by using the electric DC motor model with torque constant k_m. By using $I = \frac{T_{mot}}{k_m}$, $U = \dot{\varphi}_{mot} \cdot k_m + I \cdot R_{mot}$ and the gearbox efficiency η_{gear}, electric motor power results in

$$P_{el} = \frac{T_{mot}}{\eta_{gear}} \cdot \varphi_{mot} + \left(\frac{T_{mot}}{\eta_{gear} \cdot k_m}\right)^2 \cdot R_{mot}. \tag{2}$$

To keep the geometry simple, the curved foot is designed as a circle segment with constant radius. To be able to use Olympic weight discs as payload, the payload attachment point needs to be higher than 225 mm above the ground. Together with the finding from CHIARO which indicates a horizontal upper body to be optimal, the geometry shown in Fig. 1(A) with the parameter set shown in Tab. I resulted.

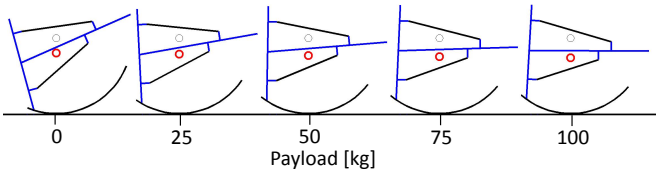

Fig. 2. Illustration of the body posture depending on the payload. The red circle marks the center of mass of the robot, the black circle represents the center of the foot circle.

B. Payload Mass and Attachment

To be able to compare the robots performance with human walking, we chose a maximum payload mass of 100 kg. Together with the robot, these 100 kg allow to cover a wide range from a child (30 kg) up to a heavy adult (130 kg). To simplify simulation and experiments we use one single payload attachment point and to minimize impact losses, the payload is attached on the upper body. The payload is able to rotate freely around the z-axis, which allows for neglecting its rotational inertia which simplifies the overall analysis.

Due to high mechanical stress resulting by the payload, the lower body and foot need a certain material usage which results in a lower body weight about 13 kg and a CoM_2 close to the hip joint. Therefore, the empty robot without payload leans backward as shown in 2) (left). With a payload attachment point slightly in front of the robot CoM, the robot leans more and more forward with increasing payload. Over the majority of the payload range, this results in a nearly horizontal body posture and the negative influence of the upwards/downwards posture at minimum payload remains manageable.

III. SIMULATION SETUP

To quantify the performance of the system in terms of energy consumption, we consider the Cost of Transportation (CoT)

$$CoT_{el} = \frac{\int P_{el} \cdot ds}{m \cdot g \cdot s} \tag{3}$$

as a cost function, which indicates the electric energy spent per robot weight $m \cdot g$ and distance travelled s.

The simulation as well as the real robot are clock torque controlled without any sensory feedback. All stabilization around the z-Axis, which was the main topic of our studies with CHIARO, is done within the mechanics. The stabilization around the x-axis of the experimental platform is achieved mechanically too by using two foot plates with a distance of 0.25 m in z-direction.

Due to ground contact interactions, namely friction and impact forces, the robot can be described as a hybrid dynamical system. We formulated the equations as a so called "Linear Complementarity Problem" by using the the approach provided in [16]. For our robot, we implemented a time stepping algorithm in order to solve the described system numerically. The curved foot was discretized by placing 78 contact points uniformly on the foot disc. The result of every numerical iteration step are the ground reaction

TABLE II

STATE VARIABLE RANGE FOR BOUNDED INPUT

	Simulation, $A_{mot} = [0..500]Nm$	**Experiment** $A_{mot} = [0..75]Nm$
Forward Speed $\dot{q}_1$	[-0.35..2.32]m/s	[0.07..0.83]m/s
CoM Height q_2	[0.23..49]m	[0.25..0.38]m
Lower leg Angle q_3	[0.33..2.36]rad	[0.33..1.89]rad
Upper leg Angle q_4	[-0.72..0.52]rad	[-0.27..0.12]rad

forces for all foot points below ground level (usually one or two). The ground contact forces of the first iteration of each stance phase thereby represent the vertical impact forces. The maximum simulation time step was 0.5 ms, which was lowered down to 0.025 ms during impact if necessary. The detailed implementation of the algorithm is described in [15].

Normal restitution factors, ground friction, and hip joint/motor damping, were validated using the real world prototype presented in section V. For the restitution factors, we chose them to be 0 for all contact points, which corresponds to no recovery of the kinetic energy of the unsprung mass at impact. To model the ground friction, we assumed an averaged friction coefficient of 0.23 throughout the simulation for all contact points. This coefficient was measured for the plywood foot sliding on the MDF surface of the test track. The avrage damping coefficient was determined to $1.3\,\mathrm{N\,m\,s\,rad^{-1}}$ by measuring the passive swing motion of the robot after the run. For each simulation, the initial conditions were precalculated in order to start from the robot's static equilibrium position. As a consequence, the same initial conditions as for the real world experiment could be guaranteed.

IV. SIMULATION RESULTS

As described in [15], the parallel elastic curved foot concept is able to perform stable forward gaits over a wide range of parameters. However, the transportation of additional payload with this mechanism remains challenging, since large payloads significantly change the natural dynamics of the robot. In this chapter, we analyse the behavioural changes depending on the payload and determine the optimal spring stiffness of the robot.

A. Successful Runs and Stability

Empirical findings from experiments with CHIARO and ETH Cargo show that motor torque frequency and hopping frequency are equal for all non-chaotic solutions. This simplifies the periodic analysis and allows for a simple definition of a successful run by using motor oscillation cycles. A motor oscillation cycle thereby starts and ends at positive zero crossing. Each run contains of 50 motor oscillation cycles, starting from deadlock. The breakdown phase after these 50 cycles is not considered.

Based on the motor oscillation cycles, we define a *successful run* by using the following criteria: First, the average horizontal speed of the robot CoM needs to be positive for each of the last 25 motor oscillation cycles, i.e. the robot needs to hop forward. Second, the robot needs to leave the ground for at least one iteration step during one of the last 25 motor oscillation cycles, i.e. it needs to hop. And third, the average horizontal speed of the robot CoM of the last 25 motor oscillation cycles must not differ more than 50%.

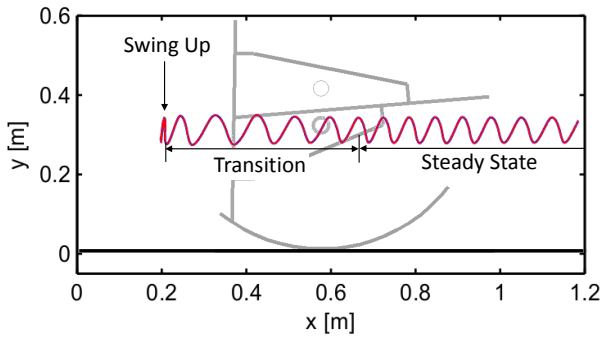

Fig. 3. Trajectory of the robot CoM (red) of a successful run to illustrate different motion phases during the run. After swinging up with no foot movement, the robot accelerates during transition phase and finally reaches steady state hopping.

By applying these criteria, the state variables of all successful runs within the bounded input parameter space remain within the bounds shown in Tab. II. This bounded-input, bounded-output stable behaviour allows for further analysis without additional investigations on stability.

B. Hopping Pattern

One successful run of the ETH Cargo is shown in Fig. 3. The run starts with the robot at rest by turning on the hip motor, which applies continuous sinusoidal torque on the hip during the whole run. In a first phase, the upper body swings up while the lower body still remains in place. As soon as the swing energy of the system is large enough, the robot enters transition phase where it accelerates forward. After 4-8 hops, it reaches steady state hopping. Here the acceleration is completed and the motion variables become periodic.

The hopping pattern during steady state hopping is shown in detail in Fig. 4. Over the whole range of motor amplitude, frequency and robot payload, this pattern remains basically the same for all successful runs and can be described as follows: At touchdown, the robot touches the ground with the curved foot. During stance phase, the foot is slipping and rolling forward while the hip joint first bends and then flexes up to lift off. During flight phase, the hip bends again while the robot swings back in landing position. Usually 2/3 of the distance of one step is travelled rolling while the remaining 1/3 is travelled flying.

C. Joint Stiffness

The natural frequency of the ETH Cargo mainly depends on its upper body mass m_1, the distance of the upper body CoM from the hip joint and spring stiffness in the hip joint c. If we attach payload at a fixed point on the upper body, the robots mass increases while lever and stiffness remain the same. As a result, the natural frequency decreases.

To find the optimal stiffness of the hip joint, we ran three sets of simulations for three different joint stiffnesses $c = [1100, 2200, 4400]Nm/rad$ at $m_p = 100kg$. For each

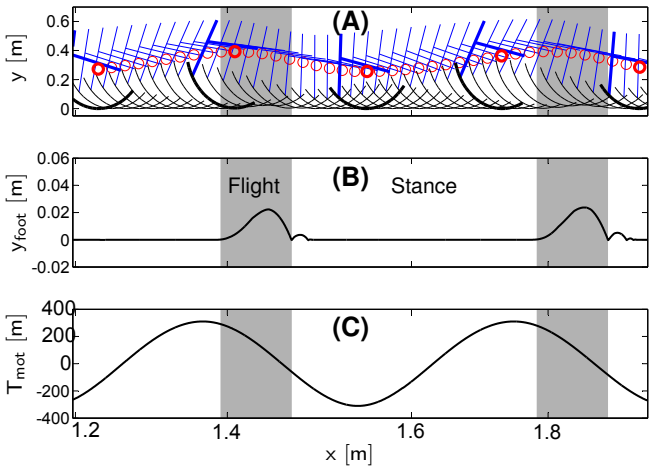

Fig. 4. Illustration of the hopping pattern with the flight phase highlighted in grey. **(A)** Motion capture series of the simulated robot. Upper and lower body are in blue and the foot circle in black. The red circle marks the CoM of the system. **(B)** Foot height y_{Foot} which describes the minimum distance between the foot and the ground. **(C)** Output torque $T_M(t)$ of the parallel joint motor.

stiffness, we ran a set of $m \cdot n$ simulations for every combination of m amplitudes $A_T \in [0..500]Nm$ and n frequencies $\omega_T \in [0..10]Hz$. By filtering out the unsuccessful runs, according to the definition in IV-A, the amount of solutions was reduced afterwards by about 90%.

The runs are displayed in Fig. 5. Every successful run with a $CoT_{el} < 3$ is displayed as a grey patch in the amplitude-frequency-plane. All unsuccessful runs and successful runs with a $CoT_{el} > 3$ are not displayed. The minimum CoT_{el} for each spring stiffness is highlighted. One can see that the general "shape" of the solution plane remains the same for the three stiffnesses and consists of three main regions. First a horizontal region around the natural frequency of the robot, which extends to a majority of the possible amplitudes and is tilted slightly downwards with increasing amplitude. This region contains solutions where the robot hops close to natural frequency with one hop per motor oscillation cycle. This region contains both very repetitive solutions where the parameters are nearly identical for each motor oscillation cycle and more unsteady solutions. Also, the best CoT_{el} can be found in this region. The second region looks similar to the first and lies around double the natural frequency. In this region, not every motor oscillation cycle leads to a hop. The third region finally is a diagonal area through the whole plane where the robot follows the actuator frequency in very short hops.

From Fig. 5, one can see that the number of parameter combinations that lead to successful runs increases with the spring stiffness. This indicates that a higher spring stiffness leads to larger robustness against parameter changes. On the other hand, a lower stiffness seems to feature better CoT_{el}. To finally decide for one stiffness, we considered the angular deflection at the hip joint. On the one hand, we wanted the system to be as soft as possible to lower the stress on the robot mechanics during stance and to benefit from the

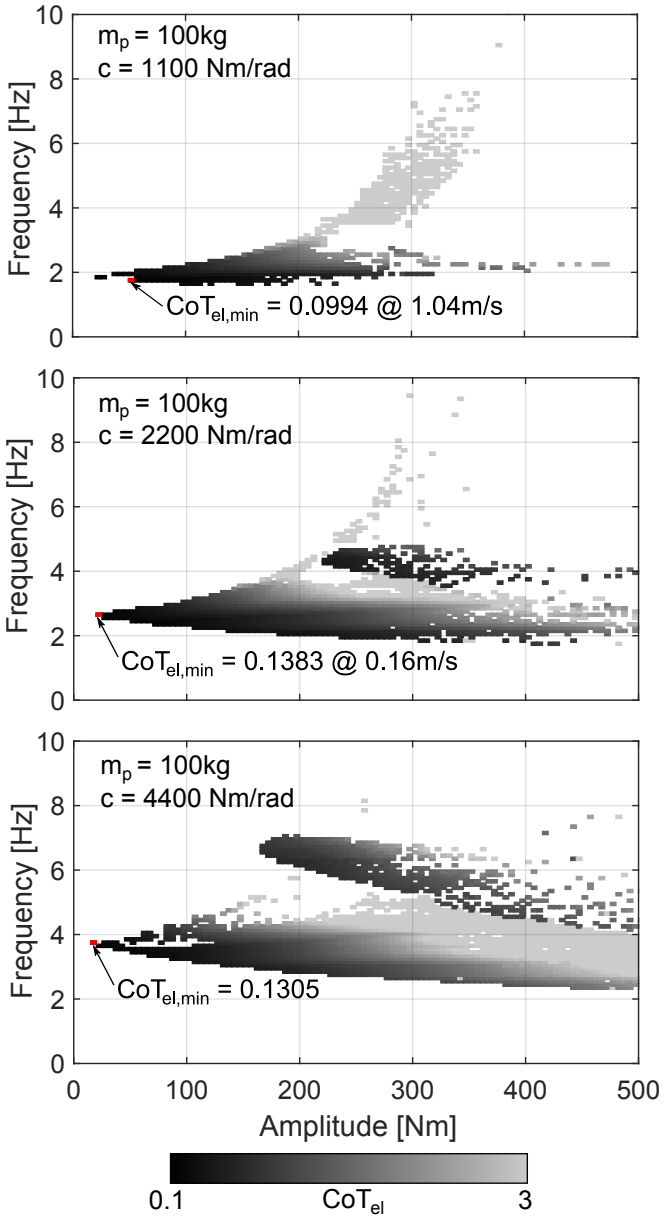

Fig. 5. CoT_{el} in simulation for $m_p = 100kg$ payload and three different spring stiffnesses $c = [1100, 2200, 4400]Nm/rad$ over the whole amplitude and frequency range. The location of the best CoT_{el} with corresponding forward speed is highlighted in red.

lower CoT_{el}. On the other hand, the angular deflection at the hip joint should remain below ± 0.5236 rad to allow for a linearization of the system for further analysis. With a deflection from -0.3611 rad to 0.0774 rad, the system with $c_{rot} = 2200\,\mathrm{N\,m\,rad^{-1}}$ fulfils the requirements.

V. DESIGN OF THE EXPERIMENTAL PLATFORM

The experimental platform ETH Cargo is shown in Fig. 6. Upper and lower body are build using a modular system based on 50 mm aluminium tubes and custom aluminium clamping braces for joints, payload and spring attachment and tube connectors. This enables for quick adaptation to new geometries without the need for manufacturing new parts.

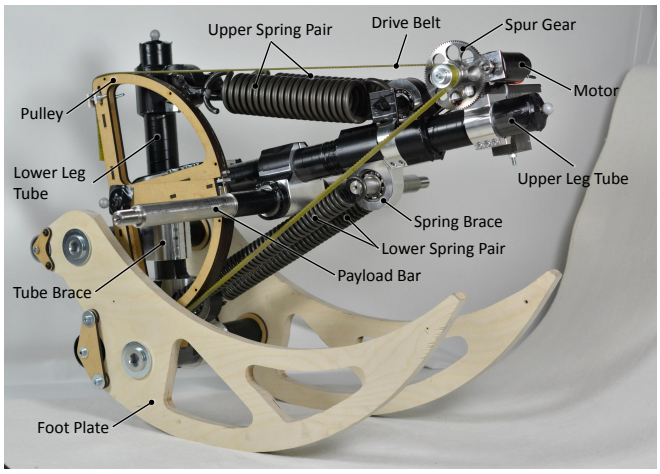

Fig. 6. Picture of the prototype of ETH Cargo used for the experiments. All parameters are identical to the model used for the simulations.

The rotational spring on the hip joint is realized by using two tension spring pairs instead of a torsional spring (see Fig. 1 (B) and Fig. 6). This allows for quick adjustment of the stiffness by changing the spring levers. Within the work range, this setup approximates the torque spring setup with errors less than 2% . Upper and lower spring were realized as spring pairs and all shafts are supported with ball bearings to minimize losses.

Since the range of lower leg angles q_4 is limited according to Tab. II, the two foot plates are designed as circle segments made from 21 mm plywood with a collateral distance of 0.25 m. For the payload, we chose commercial weight discs because of their good availability and easy handling. The whole robot was dimensioned to withstand the full tension of the upper springs (7522 N) with a safety margin > 2. The two-stage gears of the motor consist of a 16 mm drive belt (1st stage) and a spur gear (2nd stage) with a total gear reduction of 1:100 Due to the drive belt stage, the motor can be placed flexibly on the upper body and small angle errors within the stage are balanced. The motor, a Maxon RE40/24V is torque controlled using a MAXON EPOS 70/10 and a PC with Matlab and can provide a Hip torque up to 75 N m. For stand-alone runs, the ETH Cargo can be equipped with an on-board controller and batteries. Absent any inertial sensing on the ETH Cargo, we used an OptiTrack optical tracking system to record the robot's position and orientation.

VI. EXPERIMENTAL RESULTS

To verify the simulation model and to determine the CoT_{el} for different payloads, we ran two real world experiments. The setup for the experiments is build analogue to the simulations with 50 motor oscillation cycles per run. Hopping was detected acoustical since even small hopping heights of 1 mm produce clearly audible impacts.

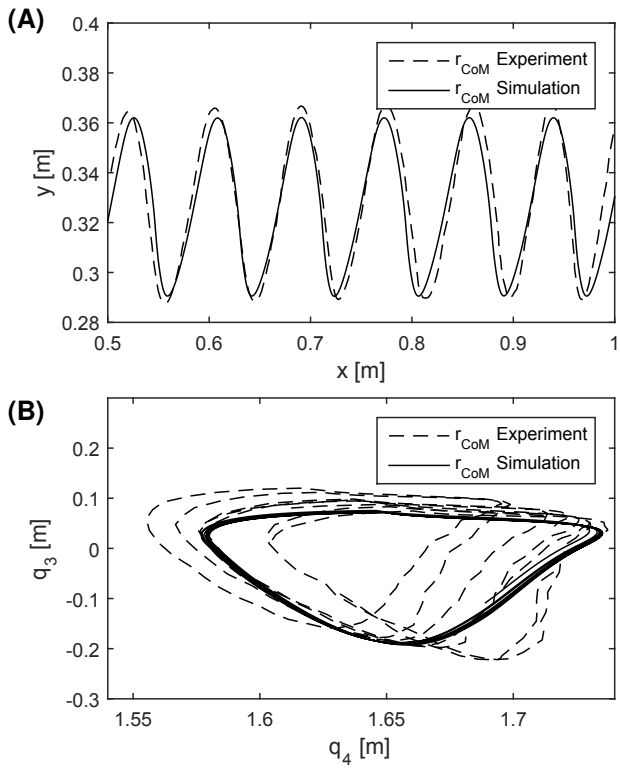

Fig. 7. (A) Simulated and experimental hip trajectory for 6 motor oscillation cycles for $m_p = 100$ kg, $A_{mot} = 35$ N m and $f_{mot} = 2.5$ Hz. (B) Upper body angle vs. lower body angle for the same run.

A. Validation of the Simulation Model

In a first experiment, we performed several experimental runs and recorded the motion data. In parallel, we simulated the runs with identical parameter sets. Fig. 7 shows the CoM trajectory and the foot and hip angle for one of these runs. As for all the other runs, simulation and experiment match adequately.

B. Efficiency for Varying Payload

In the second experiment we explored the CoT_{el} for different payloads between 0 and 100 kg. For the simulation, we considered 9 different payloads in 12.5 kg-steps. For each payload, we simulated mn runs with m different torque amplitudes and n different frequencies of the motor. Due to torque limitations of the actuator, the simulated and experimental amplitude range was limited to $A_{mot} = [0..75]Nm$. After simulation, the unsuccessful runs were filtered out. Out of the remaining solutions, the one with the smallest CoT_{el} was chosen for each payload. For the experiments, we applied the same procedure for 5 payloads in 25 kg-steps. To test the simulation, we explored a 5x5 amplitude/frequency area around the best simulation CoT_{el}. It turned out that the simulation is able to predict the amplitude and frequency for best CoT_{el} with below 5% deviation. The run at best experimental CoT_{el} was then repeated 5 times for each payload. The results of this analysis are shown in Fig. 8.

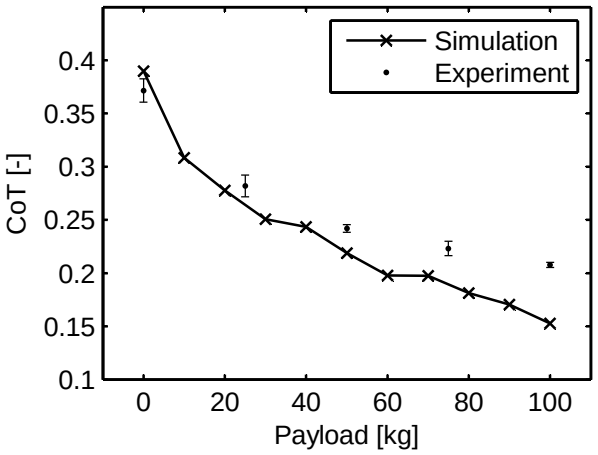

Fig. 8. Best simulated and experimental CoT_{el} for payloads between 0 and 100 kg.

As a first observation, the CoT_{el} drops with increasing payload for simulation and experiment. This can be first explained by looking at the ratio between the "empty" robot mass and the payload. The heavier the payload, the smaller the empty robot mass becomes relatively, and therefore the relative impact losses drop too. And second, the spring stiffness relative to the payload drops with increasing payload. As shown in section IV-C, a lower relative spring stiffness leads to lower CoT_{el}. In contrast to the simulation data, the decrease of the experimental CoT_{el} flatter. We suppose the non modelled internal damping of the wooden drive belt pulley and the damping of the wooden floor of the experimental track. This effects needs further investigation.

VII. CONCLUSION

This paper investigated a novel one legged payload carrier that takes advantage of parallel elastic actuation. The system is clock torque controlled, all stabilization is done mechanically. By keeping the experimental platform as simple as possible, we were able to accurately describe the system with a small number of parameters, which leads to a good match between simulated and experimental data. We successfully demonstrated payload transportation between 0 and 100 kg and a minimum CoT_{el} close to 0.2 under experimental conditions. The mechanics need no adaptation to different payloads, since any corrections can be done by varying torque amplitude and frequency of the hip motor.

At the same bodyweight and forward speed, the ETH Cargo features a better CoT than a walking human and we think that it has the potential to further explore the general minimum CoT for legged machines. In addition, it is one of the simplest machines that is able to swing its leg forward, and therefore can hop freely without external support. This is in contrast to today's most advanced SLIP designs [8],[17] which feature no swing leg behaviour, even when the overall design is pretty similar to the ETH Cargo [7]. One challenge for the future is therefore to close the gap between the powerful analytic SLIP models and the freely hopping ETH Cargo.

REFERENCES

[1] Collins, S., Ruina, A., Tedrake, R., Wisse, M. "Efficient bipedal robots based on passive dynamic walkers," *Science 307*, 2005, pp. 1082-1085.

[2] P.A. Bhounsule, J. Cortell and A. Ruina, "Design and Control of Ranger: An Energy Efficient, Dynamic Walking Robot," in *Proc. of the Fifteenth Int. Conf. on Climbing and Walking Robots and the Support Technologies for Mobile Machines (CLAWAR 2012)*, 23 ? 26 July 2012, Baltimore, MD, USA.

[3] M. Buehler, A. Cocosco, K. Yamazaki and R. Battaglia, "Stable open loop walking in quadruped robots with stick legs", in *Proc. of the 1999 IEEE Int. Conf. on Robotics & Automation (ICRA 1999),* May 1999, Detroit, Michigan, USA.

[4] M. Ahmadi and M. Buehler, "Controlled Passive Dynamic Running Experiments With the ARL-Monopod II," in *IEEE Trans. on Rob.*, Vol. 22, No. 5, 2006, pp. 974-986.

[5] S. Kim,J.E. Clark and M.R. Cutkosky, "iSprawl: Design and Tuning for High-speed Autonomous Open-loop Running", in *The International Journal of Robotics Research*, Vol. 25, No. 9, September 2006, pp. 903-912.

[6] J.Y. Jun and J.E. Clark, "A Reduced-Order Dynamical Model for Running with Curved Legs", in *Proc. of the 2012 IEEE Int. Conf. on Robotics and Automation (ICRA),* May 14-18, 2012, RiverCentre, Saint Paul, Minnesota, USA.

[7] KJ Huang, CK Huang and PC Lin, "A simple running model with rolling contact and its role as a template for dynamic locomotion on a hexapod robot," in *Bioinspir. Biomim.*, Vol. 9, No. 4, 2014

[8] J. Seipel and P. Holmes, "A Simple Model for Clock-Actuated Legged Locomotion," in *Regular and Chaotic Dynamics,*, Vol. 12, No. 5, 2007, pp. 502-520.

[9] M.H. Raibert, "Legged Robots That Balance", Cambridge, MA, USA: MIT Press, 1986, Print.

[10] U. Mettin, P.X. LaHera, L.B. Freidovich and A.S. Shiriaev, "Parallel Elastic Actuators as a Control Tool for Preplanned Trajectories of Underactuated Mechanical Systems", in *Int. Journal of Robotics Research*, 2010.

[11] G. A. Folkertsma, S. Kim, and S. Stramigioli, "Parallel stiffness in a bounding quadruped with flexible spine", in *IEEE/RSJ Int. Conf. on Intelligent Robots and Systems (IROS)*, Vilamoura, Algarve, Portugal, 2012, pp. 2210-2215.

[12] M. Grimmer, M. Eslamy, S. Gliech and A. Seyfarth, "A Comparison of Parallel- and Series Elastic Elements in an actuator for Mimicking Human Ankle Joint in Walking and Running", in *IEEE Int. Conf. on Robotics and Automation (ICRA)*, RiverCentre, Saint Paul, Minnesota, USA, 2012, pp. 2463-2470.

[13] M. Khoramshahi, A. Parsa, A. Ijspeert and M. N. Ahmadabadi, "Natural Dynamics Modification for Energy Efficiency: A Data-driven Parallel Compliance Design Method", in *2014 IEEE Int. Conf. on Robotics & Automation (ICRA)*, Hong Kong Convention and Exhibition Center May 31 - June 7, 2014. Hong Kong, China.

[14] M.D. Berkemeier and R.S. Fearing, "Sliding and Hopping Gaits for the Underactuated Acrobot", in *IEEE Transactions on Robotics and Automation*, Vol. 14, No. 4, AUGUST 1998.

[15] F. Guenther, F. Giardina and F. Iida, "Self-stable one-legged hopping using a curved foot," in *Proc. of the 2014 IEEE Int. Conf. on Robotics and Automation (ICRA 2014),* 31 May-6 June 2014, Hong Kong, China, 5133-5138.

[16] C. Glocker and C. Studer, "Formulation and Preparation for Numerical Evaluation of Linear Complementarity Systems," in *Multibody System Dynamics*, Springer-Verlag 2005, pp. 447-463.

[17] Z. Shen and J. Seipel, "Towards the Understanding of Hip Torque and Leg Damping Effects on Model Stability", in *Proc. of the ASME 2012 Int. Design Engineering Technical Conferences & Computers and Information in Engineering Conference (IDETC/CIE 2012),* August 12-15, 2012, Chicago, IL, USA.